

Accepted Manuscript

Full Length Article

Inhibitive effect of sodium (E)-4-(4-nitrobenzylideneamino)benzoate on the corrosion of some metals in sodium chloride solution

M. Talebian, K. Raeissi, M. Atapour, B.M. Fernández-Pérez, Z. Salarvand, S. Meghdadi, M. Amirnasr, R.M. Souto

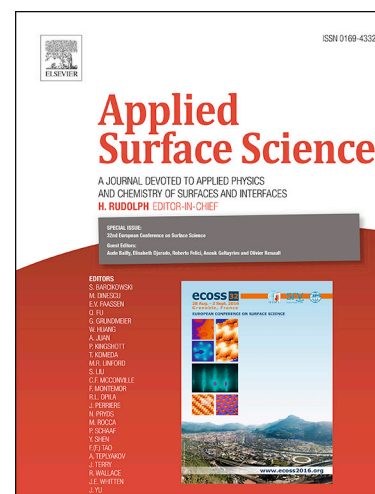
PII: S0169-4332(18)31024-9
DOI: <https://doi.org/10.1016/j.apsusc.2018.04.073>
Reference: APSUSC 39072

To appear in: *Applied Surface Science*

Received Date: 13 November 2017
Revised Date: 1 March 2018
Accepted Date: 7 April 2018

Please cite this article as: M. Talebian, K. Raeissi, M. Atapour, B.M. Fernández-Pérez, Z. Salarvand, S. Meghdadi, M. Amirnasr, R.M. Souto, Inhibitive effect of sodium (E)-4-(4-nitrobenzylideneamino)benzoate on the corrosion of some metals in sodium chloride solution, *Applied Surface Science* (2018), doi: <https://doi.org/10.1016/j.apsusc.2018.04.073>

This is a PDF file of an unedited manuscript that has been accepted for publication. As a service to our customers we are providing this early version of the manuscript. The manuscript will undergo copyediting, typesetting, and review of the resulting proof before it is published in its final form. Please note that during the production process errors may be discovered which could affect the content, and all legal disclaimers that apply to the journal pertain.



Inhibitive effect of sodium (E)-4-(4-nitrobenzylideneamino)benzoate on the corrosion of some metals in sodium chloride solution

M. Talebian¹, K. Raeissi^{1,*}, M. Atapour¹, B.M. Fernández-Pérez², Z. Salarvand³, S. Meghdadi³, M. Amirnasr³, R.M. Souto^{2,4,*}

¹ *Department of Materials Engineering, Isfahan University of Technology, Isfahan 84156-83111, Iran*

² *Department of Chemistry, Universidad de La Laguna, Avda. Astrofísico Francisco Sánchez s/n, E-38205 La Laguna (Tenerife), Canary Islands, Spain*

³ *Department of Chemistry, Isfahan University of Technology, Isfahan 84156-83111, Iran*

⁴ *Institute of Material Science and Nanotechnology, Universidad de La Laguna, P.O. Box 456, E-38200 La Laguna (Tenerife), Canary Islands, Spain*

*Corresponding authors:

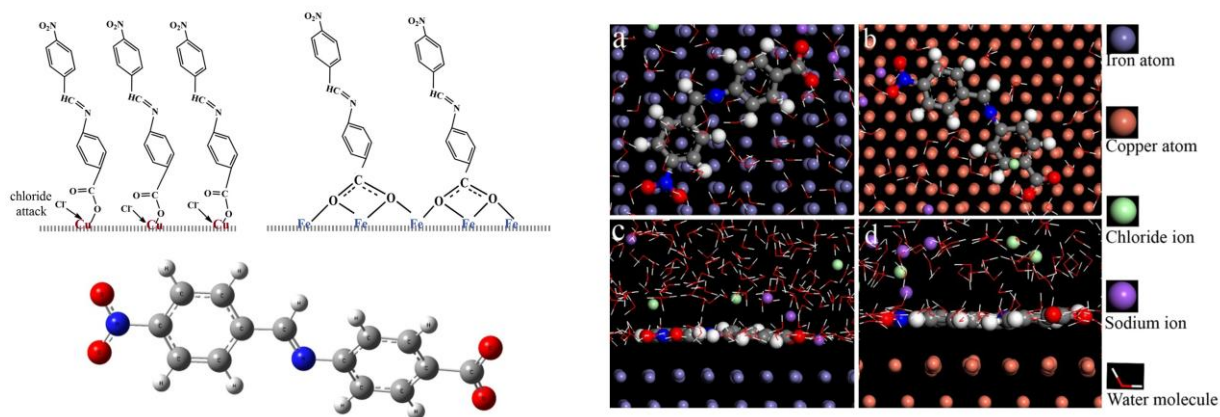
R.M. Souto, e-mail: rsouto@ull.es

K. Raeissi, e-mail: k_raeissi@cc.iut.ac.ir

Highlights:

- SNBB inhibits Fe and steel corrosion at OCP and mild anodic polarizations.
- SVET maps do not show surface reactivity on Fe and steel in the presence of SNBB.
- SNBB forms a stable complex with iron through a bidentate O, O-chelate mode.
- A heavy and highly hydrophobic complex forms on Fe and steel surface by SNBB.
- Rotation of monohapto-SNBB around Cu-O bond leads to easy detachment from Cu.

Graphical abstract

**Abstract**

The inhibition performance of a novel anionic carboxylic Schiff base, sodium (E)-4-(4-nitrobenzylideneamino)benzoate (SNBB), was investigated for various metals, namely low carbon steel F111, pure iron and copper, in neutral 10 mM NaCl solution. Potentiodynamic polarization, scanning vibrating electrode technique (SVET), quantum chemical (QC) calculation, and molecular dynamics (MD) simulation were employed. The potentiodynamic polarization data showed that SNBB acts as an effective corrosion inhibitor for both iron and F111 steel, but it is not effective for the copper. In situ spatially-resolved SVET maps evidenced a major change in surface reactivity for Fe and F111 steel immersed in 10 mM aqueous solution in the absence and in the presence of SNBB. Featureless ionic current density distributions were recorded in the presence of SNBB at both their spontaneous open circuit potential (OCP) and under mild anodic polarization conditions, while major ionic flows were monitored above the metals in the absence of SNBB. On the basis of computer simulations, it is proposed that SNBB produces a stable chelate film on iron and steel surfaces that accounts for the good corrosion

inhibition efficiency observed. The different inhibition efficiencies of SNBB molecules on the iron and copper was attributed to the special chemical structure of SNBB molecule and its different chelation ability with the released metal ions on the metal surface. The QC calculations also confirmed the high corrosion inhibition efficiency of SNBB. The MD simulation indicated higher binding energy of SNBB on iron surface compared to that of copper surface. The interaction mode of SNBB on iron and F111 steel surfaces corresponds to a mixed chemical and physical adsorption, and it obeys the Langmuir isotherm.

Keywords: Iron; Copper; Steel; Scanning Vibrating Electrode Technique; Polarization; Modelling studies; Corrosion inhibition.

1. Introduction

Corrosion is one of the most devastating problems faced in modern technology and plays an important role in various industrial fields. The use of corrosion inhibitors is a practical and effective procedure to minimize the corrosive attack on metals, and major effort is devoted to the development of more efficient corrosion inhibitors [1,2]. As result, a rather large number of organic compounds possessing electronegative heteroatoms such as P, S, N and O in their structures, or containing double or triple bonds and aromatic rings, have been proposed to protect different metals including pure iron [3,4], carbon steel [5,6], and copper [1,7].

Although experimental methods such as weight loss and conventional electrochemical measurements are the most traditional and simple ways to test inhibitors, these methods can only provide an average response on the reactivity of whole metal surface, and they implicitly assume that the electrochemical behavior at the metal/electrolyte interface is uniform. Unfortunately, corrosion inhibition is a complex process, and the inhibitor molecules must interact with the local micrometric and submicrometric cells developed on the reactive metal surface. Therefore, a comprehensive understanding of inhibition mechanisms requires the analysis of spatially-resolved data obtained in those scales [8,9]. Recently, the application of scanning microelectrochemical techniques, that are operated in situ, have opened new avenues for the investigation of the corrosion mechanisms in aqueous environments in general [10,11], and of corrosion inhibition in particular [11]. Among them, the scanning vibrating electrode technique (SVET) is a powerful microelectrochemical method that assesses corrosion phenomena by measuring the ionic fluxes in aqueous solutions produced by the corrosion reactions using a vibrating microelectrode [12]. Although the SVET has been mostly employed to measure local potential gradients originated by electrically-connected dissimilar metals [13-15] or inclusions in

alloys [16,17], and it is currently employed in the investigation of several corrosion processes ranging from coated metals [9,18-20], to corrosion inhibition [21-25]. However, these experimental measurements are costly, time consuming and sometimes unable to reveal the complete inhibition mechanisms [26,27].

With the development of sophisticated software and hardware related to computational support systems, computer simulation has been explored for investigating the complex systems in a corrosion process and predicting the relative inhibition efficiencies. In particular, quantum chemical (QC) studies using density functional theory (DFT) were conducted to explore the relationship between the molecular properties of the inhibitors and their corrosion inhibition efficiencies [28-30]. However, it was observed that only the modeling of an experiment can provide the actual interaction between corrosion inhibitors and metal surfaces. As a result, the QC calculations and molecular dynamics (MD) simulation can be used as a comprehensive technique for finding the corrosion inhibition mechanism [6,31]. Moreover, since there is a large number of alloys and metal combinations used simultaneously in the same construction in different engineering fields, the effect of corrosion inhibitors on various metals must be investigated as well [32].

The aim of this contribution is to study the inhibitive effect of a new anionic carboxylic Schiff base, sodium (E)-4-(4-nitrobenzylideneamino)benzoate (SNBB), on the corrosion behavior of various materials, namely low carbon steel F111, pure iron and copper, in order to explore its performance as a general corrosion inhibitor. Recently, we synthesized and characterized this compound with regards to the inhibition of the pitting corrosion of 304 stainless steel in neutral chloride solution [33]. An experimental multiscale electrochemical approach, comprising both conventional electrochemical techniques and spatially-resolved

microelectrochemical characterization by SVET, was employed. In addition, QC calculations based on DFT and MD simulations were applied to investigate the mechanism of corrosion inhibition and the interaction between the inhibitor molecules and the metal surfaces.

2. Experimental procedures

2.1. Preparation of samples, inhibitor and electrolytes

Three different metal samples were considered in this study, namely pure iron and copper, and a low alloy carbon steel (grade F111) with composition (wt.%): C 0.042, Si 0.042, Mo 0.005, Al 0.041, Mn 0.208, Co 0.005, Cu 0.023, Ni 0.005, Ti 0.005, Cr 0.015, and Fe balance. For conventional electrochemical testing, the specimens were soldered to polymer-coated Cu wires for electrical connection, and then, mounted in an epoxy resin to provide a flat surface for exposure to the test solution. Alternately, for SVET tests, iron and copper wires (of about 0.7 mm diameter) supplied by Goodfellow (Cambridge, United Kingdom), were employed instead. They were mounted in epoxy resin, so that only their cross sections could be exposed to the test solution. The two wires were spaced by 1 mm. In the case of the F111 steel, a sheet with the thickness of 1 mm was cut into strips of 60 mm \times 3 mm in length and width, respectively. These strips were then embedded vertically in the insulating resin. To facilitate electrical connections required for doing potentiostatic polarization, either the pure metal wires and the steel strips were allowed to protrude at the rear of the mount. Prior to conducting the experimental measurements, the electrode surface area was ground using silicon carbide paper ranging down to 4000 grit, and then rinsed with Millipore deionized water and acetone, and finally dried in air flow.

Reagents of analytical grade and deionized water (Milli-Q[®] ultrapure water quality, resistivity 18.2 M Ω cm) were employed to prepare the aqueous test solution (10 mM NaCl). The studied inhibitor, sodium (E)-4-(4-nitrobenzylideneamino)benzoate (SNBB) was synthesized according to the procedure described elsewhere [33], and its molecular structure is shown in Figure 1. Inhibitor-containing solutions were prepared with different concentrations of the SNBB ranging from 1 to 10 mM in the 10 mM NaCl test electrolyte.

2.2. Conventional electrochemical measurements

Conventional electrochemical measurements were performed in a conventional three-electrode cell kit using a computer-controlled Princeton Applied Research potentiostat/galvanostat model PARSTAT 2263. The three-electrode configuration was completed using an Ag/AgCl/(3 M) KCl reference electrode, and a platinum ring as counter electrode. Firstly, the metal samples were left unpolarized in the test solution for 1 h to spontaneously attain an almost stationary open circuit potential (OCP) value. The potentiodynamic polarization data were recorded at a scan rate of 1 mV/s by sweeping the potential from -250 mV vs. OCP toward more positive potentials until the current density exceeded either 10 $\mu\text{A}/\text{cm}^2$ for pure iron and F111 steel, or 100 $\mu\text{A}/\text{cm}^2$ for pure copper. All the electrochemical experiments were performed in quiescent condition at the laboratory temperature (~25 °C).

2.3. SVET operation

The SVET device employed in this work was a setup manufactured by Applicable Electronics Inc. (Forestdale, MA, USA) and controlled by dedicated software. The sensing

probes were 10 μm Pt-Ir (80%-20%) wires insulated by paralene C[®] and arced at the tip to expose the metal. To produce a spherical platinum black deposit of 10-20 μm diameter, the wires were then platinized. A video camera coupled with an optical microscope was used to establish the distance between probe and sample and also to follow the movement of the electrode tip vibrating over the sample during measurements. The mounted samples were surrounded laterally by sellotape to create a small container on the specimen under study, thus the electrolyte covered the specimen by a ca. 8 mm liquid column. The electrochemical cell for SVET operation was completed by using a spherical platinized probe and a Pt wire as reference electrode. A reference measurement with the microelectrode away from the active area was subtracted from the values measured during the scan. The measurements were made with the probe vibrating in a plane perpendicular to the sample at an amplitude of 10 μm . The mean distance between the microelectrode and the sample surface was 50 μm .

The SVET tests were carried out at ambient temperature (nominally 25 °C) in naturally aerated 10 mM NaCl aqueous solution. This solution was chosen to make a compromise between a sufficiently low conductivity electrolyte and enough chemical aggressiveness to satisfactorily resolve the potential gradients in the electrolyte resulting from the corrosion reactions on the metal, and to distinguish the differences in electrochemical activity between inhibited and uninhibited surfaces following the procedure described in refs. [23,34]. Although most experiments were performed at the corresponding OCP value, the surface of F111 steel was also examined under anodic polarization at -0.10 V vs. Ag/AgCl/(3 M) KCl to promote corrosion attack. In order to apply the potentiostatic polarization condition to the metal sample, an Ag/AgCl/(3 M) KCl reference electrode and a platinum ring counter electrode were introduced into the electrochemical cell. In this configuration, the exposed metal sample was connected as

the working electrode (WE). Electrochemical control was carried out using a potentiostat model 283 from EG&G Instruments (Princeton Applied Research, Oak Ridge, TN, USA).

2.4. Quantum chemical calculations

Quantum chemical (QC) calculations were performed by DFT methods. All calculations were done with *Gaussian 09* software using the hybrid *B3LYP* exchange-correlation functional and the *6-311⁺⁺G(dp)* basis sets [35]. Based on these calculations, geometric optimization of the SNBB molecule was done, and key parameters were determined, namely the energy of the highest occupied molecular orbital (E_{HOMO}), the energy of the lowest unoccupied molecular orbital (E_{LUMO}), the energy band gap (ΔE) between LUMO and HOMO, the dipole moment (μ), and the fractional number of electrons transferred (ΔN) to the inhibitor.

2.5. Molecular dynamics simulation

Molecular dynamics (MD) simulations are a modern tool employed to obtain more information about the adsorption of the inhibitor molecules on metal surfaces at molecular level [36-38]. The adsorption processes of the SNBB molecule on iron and copper surfaces were investigated by MD simulation using *Material Studio 6.0* software from Accelrys Inc. Since the most densely packed planes of the crystalline metals can be considered as the most stable, it is usual to choose these planes as the metal surfaces in MD simulations [6,39,40]. The simulations for iron were made by taking the Fe (110) crystal surface in a simulation box of dimensions 3.44 nm \times 4.05 nm \times 5.34 nm. Analogously, the Cu (111) crystal orientation surface in a simulation box of dimensions 4.09 nm \times 4.63 nm \times 5.85 nm was picked for copper. The MD simulations were carried out with periodic boundary conditions to model a representative part of the interface

devoid of any arbitrary boundary effects. Firstly, the appropriate surface was cleaved from the pure Fe or Cu crystal, and relaxed by minimizing its energy using molecular mechanics. Next, the surface areas of Fe (110) and Cu (111) were enlarged by constructing a super cell, and then a vacuum slab with zero thickness was built above these surfaces. The chemical species included in the adsorption system were 500 H₂O, 10 Na⁺, 10 Cl⁻ and 1 SNBB molecule in each case. Since the electrochemical corrosion inhibition process takes place in aqueous solution, the use of water molecules and different ions is essential [41]. Finally, the corrosion systems were produced by placing the Amorphous Cell on the super cell. Furthermore, all layers of the super cell, except the top layer, were kept fixed. The MD simulations were performed at 298.0 K (controlled by the Andersen thermostat) using a canonical ensemble (NVT) with a time step of 1.0 fs, and a simulation time of 500 ps. For the whole simulation procedure, the *COMPASS* (Condensed-phase Optimized Molecular Potentials for Atomistic Simulation Studies) force field [42] was used, because it allows the accurate and simultaneous prediction of structural, conformational, vibrational, and thermophysical properties for a broad range of chemical species, including organic molecules, metals, metal oxides, and metal halides [43].

3. Results and discussion

3.1. Conventional electrochemical measurements

The relationships between OCP values and immersion time for F111 steel, pure iron and copper upon immersion in 10 mM NaCl, both in the absence and in the presence of SNBB, were determined at 25 °C, and they are shown in Figure 2. The potential-time curves shifted to more positive potentials in the presence of SNBB, this effect being greater with increasing SNBB concentration. In addition, the effect of SNBB addition on the OCP values was more pronounced

in the case of iron and F111 steel. Since almost constant OCP values were observed after 1 h immersion for all the materials, it was decided to perform all the electrochemical and microelectrochemical tests after 1 h immersion of the metal substrates in the corresponding test solution.

Typical potentiodynamic polarization curves of F111 steel, pure iron and copper in 10 mM NaCl, in the absence and presence of different concentrations of SNBB, are shown in Figure 3. In the case of pure iron and F111 steel, the addition of SNBB produced a remarkable decrease of the corrosion current density (j_{corr}) accompanied by the establishment of a more positive corrosion potential (E_{corr}). The occurrence of a pseudo-passive region was observed in the anodic branches by increasing the SNBB concentration added to the test NaCl solution. However, the efficiency of SNBB as a corrosion inhibitor for copper was very poor under the same experimental conditions. The polarization curves shown in Figure 3c exhibited smaller changes after the addition of the inhibitor to the test solution, and even exhibited slightly more negative E_{corr} and breakdown potential values than in the inhibitor-free solution.

The Tafel extrapolation method was used to extract the relevant electrochemical parameters according to the procedures described in ref. [44], and the obtained results are given in Table 1. The surface coverage (θ_p) and the inhibition efficiency ($\eta_p\%$) values were calculated using [6]:

$$\theta_p = \frac{j_{\text{corr}}^o - j_{\text{corr}}}{j_{\text{corr}}^o} \quad (1)$$

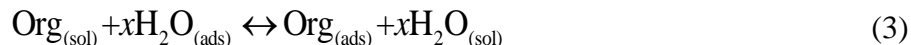
$$\eta_p \% = \theta \times 100 \quad (2)$$

where j_{corr}^o and j_{corr} represent the corrosion current densities in the absence and presence of SNBB, respectively. From the inspection of Table 1, it can be observed that the j_{corr} values

decreased for F111 steel and pure iron upon the addition of different SNBB concentrations to the 10 mM NaCl solution. It should be remarked that no significant changes in the cathodic Tafel slope (β_c) occurred either by adding or increasing the SNBB concentration. This feature indicates that the SNBB did not influence the cathodic reaction mechanism of the corrosion process. Thus, the SNBB can be regarded as anodic-type corrosion inhibitor. According to Table 1, η_p % increased with the increase of the inhibitor concentration. In the case of copper, j_{corr} and E_{corr} values were not significantly influenced by SNBB.

3.2. Adsorption isotherm

The adsorption of organic inhibitor compounds at the metal/solution interface is the first step in the corrosion inhibition mechanism of metals and alloys. The adsorption process mainly depends on the electronic characteristics of the metal surface and inhibitor, the charge and nature of the metal surface, the adsorption of the solvent and other ionic species, temperature, the electrochemical potential at the solution/interface, steric effects, and varying degrees of surface-site activity [45,46]. Two main types of interaction are responsible for bonding an inhibitor to a metal surface. Physical adsorption is a weak, non-directional interaction, and it involves electrostatic interaction between the inhibitor organic ions or dipoles and the electrically-charged metal surface [47]. The second type of interaction is chemical adsorption, which occurs by directional forces between the adsorbate and adsorbent. It involves charge sharing or charge transfer from the adsorbates to a vacant low-energy orbital of the metal surface to form a coordinate type bond [46]. Adsorption of inhibitor molecules is a quasi-substitution process where organic compounds in the aqueous phase ($\text{Org}_{(\text{sol})}$) replace water molecules at the electrode surface ($\text{H}_2\text{O}_{(\text{ads})}$) according to following reaction [6]:



where $\text{Org}_{(\text{ads})}$ is the organic inhibitor adsorbed on the metal surface, and $\text{H}_2\text{O}_{(\text{sol})}$ is the water molecule in the aqueous solution, and x (the size ratio) is the number of water molecules replaced by the organic inhibitors. In order to obtain the isotherm, a linear relation between θ_p values and the inhibitor concentration (C_{inh}) must be found. In the present study, the best fit was obtained with the Langmuir isotherm given by Eq. (4):

$$\frac{C_{\text{inh}}}{\theta_p} = \frac{1}{K_{\text{ads}}} + C_{\text{inh}} \quad (4)$$

where K_{ads} is the adsorption equilibrium constant that can be extracted from the intercept of the straight line on the C_{inh}/θ_p axis. Figure 4 shows the straight lines with slopes close to unity obtained for the interaction of SNBB with Fe and F111 steel, whereas Table 2 gives the calculated K_{ads} values for these metal-inhibitor systems. The Langmuir adsorption isotherm has been employed extensively in previous works to describe the adsorption reaction of certain extracts with steel surfaces resulting in the formation of stable chelates [48,49]. This adsorption isotherm assumes that there are fixed numbers of adsorption sites on the metal surface, and each site holds one inhibitor molecule. The standard free energy of the inhibitor adsorption (ΔG_{ads}^0) is the same for all these sites, it is independent of θ , and the adsorbed inhibitor molecules do not interact with each other [46,50]. The value of ΔG_{ads}^0 was calculated from K_{ads} using [6]:

$$\Delta G_{\text{ads}}^0 = -RT \ln(55.5 K_{\text{ads}}) \quad (5)$$

where R is the universal gas constant, T is the absolute temperature, and 55.5 is the molar concentration of water in the solution. It is commonly accepted that ΔG_{ads}^0 values equal to or less negative than -20 kJ/mol correspond to physical adsorption, whereas values around or more

negative than -40 kJ/mol are related to chemical adsorption. However, the adsorption of organic compounds on the metal surface often cannot be attributed to exclusively physical or chemical adsorption processes. It has been reported that in the case of the chemical adsorption of organic compounds, some molecules can also be adsorbed on the surface via physical adsorption [51]. By considering the values of ΔG_{ads}^0 listed in Table 2, the adsorption of the SNBB molecules on the surface of pure iron and F111 steel can be assumed to be of a mixed type of chemical and physical adsorptions.

3.3. Scanning vibrating electrode technique

The possible occurrence of localized effects on the surface of iron, copper and F111 steel exposed to an aqueous chloride-containing solution and for the corrosion inhibition performance of SNBB on these metals has been investigated in situ at the micrometric scale using SVET. The chemical reactions associated to metal dissolution and the complementary cathodic reaction cause ionic fluxes to occur in the solution adjacent to a corroding surface. These ionic fluxes can be detected by SVET. It is well known that the chemical reactions of iron in a neutral chloride-containing solution occur through half-cell reaction (6) for the anodic process, and (7) for the cathodic reaction.



Therefore, the anodic and cathodic half-cell reactions can be detected by SVET as positive and negative current densities according to the sign of the ions released in each process [15].

The local effects of SNBB responsible for the enhanced corrosion resistance of the F111 steel were effectively revealed in the recorded SVET maps. Figure 5 depicts optical images of the surface and SVET maps recorded for the F111 steel strip immersed in 0.01 M NaCl solution both in the absence and in the presence of 0.01 M SNBB. Each SVET map is plotted as both 2D and 3D graphs. The samples were kept at their corresponding OCP values in the electrolyte for 60 min prior to measuring the SVET map. As it can be seen in Figure 5a, the electrochemical activity related to ionic flow from anodic sites involved rather high current densities from a few locations on the surface in the case of the strip exposed to the SNBB-free test solution. The SVET map shows three small anodic regions on the metal surface, the most active two occurring for Y values around $3000 \mu\text{m}$ (i.e., in the upper part of the 2D-map, although these two sites could not be resolved in the optical image recorded while the vibrating tip was scanning the surface), and another less active site at Y values close to zero (cf. the corrosion spot in the lower part of the optical photograph). The rest of the exposed surface showed a rather homogeneous behaviour as the location of the cathodic half-cell reaction (see the extensive blue-colored region in the SVET images). Conversely, the SVET map recorded in the presence of 0.01 M SNBB shows only the background noise signal (Figure 5b), which is composed by a random distribution of small positive and negative spikes extending over the complete surface of the exposed steel. It should be noticed the almost 50 times smaller interval of ionic current densities covered by the color bar of Figure 5b compared to that in Figure 5a, evidencing that no ionic current signals could be resolved above the lower limit of detection in this case. These observations confirm the high corrosion efficiency conferred by SNBB to the low carbon F111 steel in the neutral NaCl solution under open circuit conditions. This inhibitive action was readily observable from the comparison of the optical micrographs taken after recording the

SVET maps in each solution. The onset of localized corrosion processes accompanied by the precipitation of corrosion products only occur for the F111 steel in the inhibitor-free NaCl solution.

In order to investigate the inhibition performance of SNBB on the corrosion behavior of F111 steel subjected to anodic polarization, the surface of F111 steel was also scanned at -0.10 V vs. Ag/AgCl/(3 M) KCl in 0.01 M NaCl solution in the absence and presence of 0.01 M of SNBB. This potential value was chosen from the comparison of the potentiodynamic polarization curves measured in the absence and in the presence of SNBB shown in Figure 2a. This polarization is positive enough to promote enhanced metal dissolution in the absence of the inhibitor, yet it lies within the passive region of the steel in the presence of the organic molecule. The SVET maps obtained for F111 steel under this anodic polarization are shown in Figure 6. Again, only background noise levels were observed in the presence of inhibitor, but, in the absence of inhibitor, the steel surface experience extensive degradation. A large number of pits were nucleated on the surface leading to metal dissolution. It must be noticed that every anodic spike in the SVET map given in Figure 6a releases more than 20 times the amount of metal ions due to the different current density amplification in the images of Figure 5a and Figure 6a. Another major difference between the SVET images of Figures 5a and 6a regards the cathodic process. No ionic fluxes corresponding to the cathodic half-cell reaction could be observed above the metal surface in the SVET image of Figure 6a, that was recorded while the steel strip was subjected to anodic polarization. This feature is consistent with the operation of an external potentiostat, which imposes any cathodic reaction to occur at the auxiliary electrode. In conclusion, the SVET results demonstrated the excellent corrosion inhibition efficiency of SNBB

for the F111 steel even under the application of anodic polarizations within the extended passive potential range conferred by this inhibitor to the metal.

Although the SVET image in Figure 6a shows a region of weak negative ionic current densities above the resin at the right side of the metal strip, this inconsistency is due to the technical limitations originating from asymmetries in the ionic currents flowing between the counter electrode and the substrate of different shapes [52]. It must be noticed that the auxiliary electrode was built as a ring that was placed adjacent to the walls of the small microelectrochemical cell used for the SVET measurements, whereas the steel sample has no circular symmetry.

A different sample configuration was employed to investigate the inhibition characteristics of iron and copper by SVET. Samples containing one wire of each metal, with 1 mm separation between them, were fabricated in order to compare their different interactions with SNBB on a single scan. Figure 7 shows representative current density maps generated by SVET for the iron and copper wires after 1 h immersion in 0.01 M NaCl in the absence and in the presence of SNBB. In the absence of the inhibitor (see Figure 7a), ionic current densities related to electrochemical activation of the metal surface were only observed above the iron surface due to the higher corrosion tendency of iron as compared to the copper in the same solution. Figure 7b shows that the electrochemical reactions are inhibited strongly in the presence of the SNBB, reaching total current values close to zero, indicating an efficient inhibition. On the other hand, no observable changes were produced on copper by the addition of SNBB to the test electrolyte.

3.4. Chemical structure and mechanism of corrosion inhibition

The corrosion process of metals and alloys in an aqueous solution consists of an anodic and a cathodic reaction as described for iron in equations (6) and (7), respectively. By combining both processes, the overall reaction for the corrosion process of iron in neutral solution would be:



Therefore, a corrosion product film consisting of $\text{Fe}(\text{OH})_2$ can be formed on the surface of iron and its alloys, although in dilute sodium chloride solutions (i.e., for NaCl contents smaller than 3 wt.%), this deposited film does not provide a protective barrier layer [53].

On the other hand, the mechanism of copper dissolution at chloride concentrations less than 1 M is [54,55]:



Similar to iron, this deposited film does not provide a protective barrier layer for copper [55].

It has been reported that carboxylic Schiff bases can form chelates with different metal ions such as iron or copper producing stable compounds [56,57]. The multiscale electrochemical characterization reported here supports that the SNBB molecule is an efficient inhibitor for iron and steel in neutral chloride-containing solution, but it does not provide effective protection to copper. The noteworthy difference between the inhibition efficiencies of SNBB on iron and copper must then relate to the coordination chemistry of these metals. The Cu^+ ion favors complex formation with carboxylic acid derivatives mainly through one of the oxygen atoms of the carboxylic functional group ($\eta^1\text{-O}_2\text{C-R}$) [58]. Moreover, considering the electroneutrality principle, further coordination of the second oxygen atom of the carboxylate group using a bidentate O, O- chelating mode is not a favorable process for Cu^+ , leaving it exposed to Cl^- attack. As result, SNBB forms a Cu-SNBB complex with the carboxylate ion in monohapto-

coordination mode (η^1 -O₂C-R), as described by reaction (11). The resulting configuration is sketched in Figure 8a. The monohapto SNBB in the Cu-SNBB complex retains its freedom of rotation around the Cu-O bond, leading to the ease of detachment from copper surface which is also enhanced by Cl⁻ ion attack.



Conversely, the SNBB molecule forms a stable complex with iron through a bidentate O, O-chelate mode using both oxygen atoms of the carboxylic functional group, forming Fe-SNBB complex with dihapto-carboxylate coordination (η^2 -O₂C-R), as described by reaction (12) and sketched in Figure 8b. This is a relatively heavy complex with high hydrophobicity characteristics and a stronger attachment to the surface of iron [59-62]. Such hydrophobic complexes favor the formation of surface compounds which promote passivation, that thickens the barrier layer to a limiting value, thus hindering water penetration and further oxide formation [63,64]. This passive layer can effectively inhibit the anodic process, resulting in lower polarization current densities (cf. Figure 3b).



3.5. Quantum chemical study

The QC method has become a common practice in corrosion inhibition studies to assist the interpretation of the experimental results and to elucidate the reaction mechanisms. This will in turn help to characterize the interactions between an inhibitor molecule and the metal surface [65]. In this context, we have performed the QC calculation to justify experimental results obtained from the electrochemical measurements in the previous sections, and to investigate the effect of SNBB electronic structure on its inhibition behavior as corrosion inhibitor. Figure 9

shows the optimized molecular structure of the inhibitor and the frontier molecular orbitals (HOMO and LUMO) obtained using the combined *B3LYP/6-311G*** methodology. The optimized geometry of SNBB molecule reveals that its structure is close to planar, a geometry that favors a strong interaction with the metal surface through its π -system (see Figure 9a). On the other hand, the HOMO density distribution given in Figure 9b is mostly localized on the carboxylic functional group ($-\text{COO}^-$), evidencing that the free electron pairs are available for nucleophilic interaction with the metal surface from this center. The negative charge of the molecule-ion is also distributed on this center. As a result, it is expected that both physisorption and chemisorption on the metal surface occur from the same region of this compound.

According to Koopman's theory [41,66-69], the ionization potential (I) and the electron affinity (A) of an inhibitor molecule are a function of the energies of the HOMO, E_{HOMO} , and the LUMO, E_{LUMO} , respectively:

$$I = -E_{\text{HOMO}} \quad (13)$$

$$A = -E_{\text{LUMO}} \quad (14)$$

The absolute electronegativity (χ), and the global hardness (η) of the inhibitor compound were calculated using the following equations:

$$\chi = \frac{I + A}{2} \quad (15)$$

$$\eta = \frac{I - A}{2} \quad (16)$$

Thus, the electrons transferred from the inhibitor to the unoccupied orbitals of metal (i.e., more precisely, the electron-donating ability, ΔN) configure another key parameter correlating the

inhibition efficiency with parameters of the molecular structure. The parameter ΔN can be determined according to:

$$\Delta N = \frac{(\chi_{\text{metal}} - \chi_{\text{inh}})}{2(\eta_{\text{metal}} + \eta_{\text{inh}})} \quad (17)$$

where χ_{metal} and χ_{inh} are the absolute electronegativities of the metal and the inhibitor, and η_{metal} and η_{inh} are the absolute hardness of the metal and the inhibitor, respectively. The values for the electronegativity of Fe^{2+} ($\chi_{\text{Fe}^{2+}} = 23.42$ eV/mol) and Cu^+ ($\chi_{\text{Cu}^+} = 14.01$ eV/mol), and their hardness ($\eta_{\text{Fe}^{2+}} = 7.24$ and $\eta_{\text{Cu}^+} = 6.28$) were taken from the literature [66-68,10]. In this way, key quantum chemical parameters were computed, namely the total energy (E_t), the energies of the HOMO (E_{HOMO}) and the LUMO (E_{LUMO}), the energy gap ΔE ($=E_{\text{HOMO}} - E_{\text{LUMO}}$), the dipole moment (μ), and the ΔN that directly influence the interaction of the inhibitor with the metal surface. These parameters are listed in Table 3.

According to the frontier molecular orbital theory, the chemical reactivity depends directly on the interaction of the HOMO and LUMO levels of the participating species (i.e., inhibitor and metal) [71]. A high energy HOMO leads to a higher electron donor ability and a low energy LUMO indicates easier electron accepting by the inhibitor. A low energy ΔE also provides an increased chemical reactivity. Thus, all these parameters can be considered as a criterion for good inhibition efficiency [69,71-75]. In comparison with the results reported in the literature (Table 4), the values of E_{HOMO} and ΔE obtained for SNBB are significantly high confirming very high degree of performance of this molecule as a corrosion inhibitor for iron and low carbon steels.

According to Lukovits and coworkers [72], the inhibition efficiency increases with increasing electron-donating ability of inhibitor to the unoccupied orbitals of metal if $\Delta N < 3.6$.

In other words, higher values of ΔN correspond to better performance of the corrosion inhibitors. But, if $\Delta N > 3.6$, the inhibition efficiency decreases with the increase in the value of ΔN [75,76]. As it is concluded from the inspection of Table 3, the results show good agreement with the experimental observations concerning inhibition efficiency of the SNBB for iron and copper that were established from the electrochemical experiments. In order to evaluate a more realistic picture of the inhibitor-surface interaction, the MD simulations are considered in the next section.

3.6. Molecular dynamics simulation

The molecular dynamics (MD) simulation approach was employed to gain more information about the adsorption behavior of SNBB on Fe and Cu surfaces. At the molecular level, the most favorable configuration of the molecules on the metal surface and the values of the adsorption ($E_{\text{adsorption}}$) and binding (E_{binding}) energies between the organic inhibitor and the metal surface can be obtained by means of the MD simulation [6,39]. The equilibrium configurations of the SNBB on the Fe(110) and Cu(111) surfaces are depicted in Figure 10. It was observed that the carboxylic functional group ($-\text{COO}^-$) of the SNBB compound adsorbed on the iron and copper surfaces at first. Then, the remaining centers of the SNBB have moved gradually close to the metal surface. Therefore, as seen in Figure 10, the SNBB molecule is adsorbed on the metal surfaces with an almost flat orientation. This parallel configuration supports the maximum contact and also the higher surface coverage. To obtain more information about the interaction of SNBB on the iron and copper surfaces (including comprehensive interaction such as physical and chemical adsorption), the values of $E_{\text{adsorption}}$ and E_{binding} between the inhibitor species and the metal surfaces were calculated using equations (18) and (19) [6,40]:

$$E_{\text{adsorption}} = E_{\text{total}} - (E_{\text{surface+solution}} + E_{\text{inhibitor+solution}}) + E_{\text{solution}} \quad (18)$$

$$E_{\text{binding}} = -E_{\text{adsorption}} \quad (19)$$

where E_{total} represents the total energy of the simulation system; $E_{\text{surface+solution}}$ is the energy of the system without the inhibitor; $E_{\text{inhibitor+solution}}$ is the energy of the system without the metal surface; and E_{solution} is the energy of the aqueous solution. The calculated adsorption and binding energies for the investigated systems are given in Table 5. The negative sign of $E_{\text{adsorption}}$ values implies that the interaction between SNBB species with the metal surface is spontaneous, and more negative values of the adsorption energy and higher values of the binding energy can be attributed to the stable and strong interaction of the inhibitor on the metal surface [77]. It is observed in Table 5 that the binding energy of SNBB on the iron surface is almost two times higher than the energy determined for the copper surface. This supports the occurrence of a more stable and stronger interaction of the SNBB on the iron surface than on the copper surface. It has been reported that the organic inhibitors with unoccupied orbitals promote the formation of a chelate on the metal surface by accepting electrons from a d-orbital of the metal during such strong adsorption process [37,49]. Therefore, the SNBB species can form a stable chelate with the iron after strong adsorption, and this leads to a good corrosion inhibition efficiency.

4. Conclusions

The inhibition characteristics of a novel anionic carboxylic Schiff base, sodium (E)-4-(4-nitrobenzylideneamino)benzoate (SNBB), on the corrosion behavior of iron, copper and F111 grade steel in chloride-containing aqueous environment was investigated using a combination of multiscale electrochemical methods and computer simulation techniques. Potentiodynamic polarization analysis provided the quantification of the inhibitor efficiency and the adsorption

mode of SNBB for each metal, whereas scanning vibrating electrode technique measurements provided spatially-resolved information of the corrosion processes by identifying anodic and cathodic site distributions on the surface. Quantum chemical calculation and molecular dynamics simulation were further applied to investigate the mechanism of corrosion inhibition and to quantify the interaction between the inhibitor molecules and the metal surface. The following conclusions are derived:

- Potentiodynamic polarization measurements supported that SNBB could act as an effective inhibitor for iron and carbon steel in neutral chloride-containing solution. The inhibition efficiency increased with the increase of SNBB concentration. The surface film formed on the surface of these materials produced a wider passive region that would break at sufficiently positive polarizations with the nucleation of corrosion pits. However, the use of SNBB as a corrosion inhibitor for copper was not efficient.
- On the basis of surface-averaging electrochemical data, the adsorption of SNBB on iron and F111 steel was found to obey the Langmuir adsorption isotherm. Subsequent thermodynamic analysis revealed that the adsorption mode was of a mixed nature (i.e., both physisorption and chemisorption should be considered in order to account for the observed behaviors).
- Spatially-resolved monitoring of the surface reactivity using SVET in situ demonstrated that a major change in the corrosion mechanism of iron and F111 steel occurs when SNBB is added to the test solution. The onset of localized corrosion sites on the exposed surface was greatly hindered as result of the interaction established between the inhibitor and the metal both under spontaneous open circuit and mild anodic polarization

conditions. This feature confirmed the successful formation of a stable chelate film on the iron surface by SNBB accounting for the observed good corrosion inhibition efficiency.

- SVET imaging of samples containing copper and iron wires in inhibitor-free solution evidenced iron oxidation would be initiated from greatly localized anodic areas of high electrochemical activity for iron dissolution. Conversely, these electrochemical reactions were inhibited when SNBB was present in the aqueous phase due to the inhibitor-containing layer formed on the iron surface.
- The difference between the inhibition efficiencies of SNBB on iron and copper surfaces could be attributed to the chemical structure of the inhibitor molecule and its different coordination modes (η^1 -O₂C-R for copper and η^2 -O₂C-R for iron) with the metallic ions present on the metal surface.
- The HOMO density distribution was mostly localized on the carboxylate functional group (-COO⁻), which provided the active site responsible for the nucleophile reaction of the inhibitor molecule with the metal surface. The QC calculation results also confirmed the experimental trends of inhibition efficiency found for the metals investigated in this work.
- The MD simulation revealed that the SNBB molecules adsorbed on the surface of iron and copper adopting a nearly parallel configuration. However, the binding energy value of SNBB on the iron surface is higher than that for the copper surface, suggesting the establishment of a more stable and stronger interaction of the SNBB compound on iron than on copper.

Acknowledgements

M. Talebian expresses his greatest gratitude to Isfahan University of Technology (IUT) for the financial support of a 6-month mobility grant to the University of La Laguna. B.M. Fernández-Pérez is grateful to the Canarian Agency for Research, Innovation and Information Society (Las Palmas de Gran Canaria, Spain) and the European Social Fund (Brussels, Belgium) for a research contract. Financial support by the IUT and by the Spanish Ministry of Economy and Competitiveness (MINECO, Madrid) and the European Regional Development Fund, under grant CTQ2016-80522-P, is gratefully acknowledged.

References

- [1] A. Kokalj, S. Peljhan, M. Finšgar, I. Milošev, What determines the inhibition effectiveness of ATA, BTAH, and BTAOH corrosion inhibitors on copper?, *Journal of the American Chemical Society*, 132 (2010) 16657-16668.
- [2] N. Chafai, S. Chafaa, K. Benbouguerra, D. Daoud, A. Hellal, M. Mehri, Synthesis, characterization and the inhibition activity of a new α -aminophosphonic derivative on the corrosion of XC48 carbon steel in 0.5 M H₂SO₄: Experimental and theoretical studies, *Journal of the Taiwan Institute of Chemical Engineers*, 70 (2017) 331-344.
- [3] A. Chetouani, B. Hammouti, A. Aouniti, N. Benchat, T. Benhadda, New synthesised pyridazine derivatives as effective inhibitors for the corrosion of pure iron in HCl medium, *Progress in Organic Coatings*, 45 (2002) 373-378.
- [4] A. Chetouani, B. Hammouti, T. Benhadda, M. Daoudi, Inhibitive action of bipyrazolic type organic compounds towards corrosion of pure iron in acidic media, *Applied Surface Science*, 249 (2005) 375-385.
- [5] R. Sadeghi Erami, M. Amirnasr, K. Raeissi, M.M. Momeni, S. Meghdadi, Multidentate Schiff bases as new and effective corrosion inhibitors for mild steel in hydrochloric acid solution: an electrochemical and quantum chemical assessment, *Journal of the Iranian Chemical Society*, 12 (2015) 2185-2197.
- [6] Z. Salarvand, M. Amirnasr, M. Talebian, K. Raeissi, S. Meghdadi, Enhanced corrosion resistance of mild steel in 1 M HCl solution by trace amount of 2-phenyl-benzothiazole

- derivatives: Experimental, quantum chemical calculations and molecular dynamics (MD) simulation studies, *Corrosion Science*, 114 (2017) 133-145.
- [7] L. Kazansky, I. Selyaninov, Y.I. Kuznetsov, Adsorption of 2-mercaptobenzothiazole on copper surface from phosphate solutions, *Applied Surface Science*, 258 (2012) 6807-6813.
- [8] R.M. Souto, B. Normand, H. Takenouti, M. Keddad, Self-healing processes in coil-coated cladding studied by the scanning vibrating electrode, *Electrochimica Acta*, 55, (2010) 4551-4557.
- [9] L. Coelho, M. Mouanga, M.-E. Druart, I. Recloux, D. Cossement, M.-G. Olivier, A SVET study of the inhibitive effects of benzotriazole and cerium chloride solely and combined on an aluminium/copper galvanic coupling model, *Corrosion Science*, 110 (2016) 143-156.
- [10] R.S. Lillard, Scanning electrode techniques for investigating near-surface solution current densities, in: *Analytical Methods in Corrosion Science and Engineering*, (P. Marcus, F. Mansfeld, Eds.), CRC Press, Boca Raton, FL, 2006, pp. 571-604.
- [11] M.B. Jensen, D.E. Tallman, Application of SECM to corrosion studies, in: *Electroanalytical Chemistry: A Series of Advances*, Vol. 24, (A.J. Bard, C.G. Zoski, Eds.), CRC Press, Boca Raton, FL, 2012, 171-286.
- [12] A.C. Bastos, M.C. Quevedo, O.V. Karavai, M.G.S. Ferreira, Review – On the application of the scanning vibrating electrode technique (SVET) to corrosion research, *Journal of The Electrochemical Society*, 164 (2017) C973-C990.
- [13] H.S. Isaacs, The measurement of the galvanic corrosion of soldered copper using the scanning vibrating electrode technique, *Corrosion Science*, 28 (1988) 547-558.

- [14] D.A. Worsley, H.N. McMurray, A. Belghazi, Determination of localised corrosion mechanisms using a scanning vibrating reference electrode technique, *Chemical Communications*, (1997) 2367-2370.
- [15] R.M. Souto, Y. González-García, A.C. Bastos, A.M. Simões, Investigating corrosion processes in the micrometric range: A SVET study of the galvanic corrosion of zinc coupled with iron, *Corrosion Science*, 49 (2007) 4568-4580.
- [16] A.J. Aldykiewicz, H.S. Isaacs, Dissolution characteristics of duplex stainless steels in acidic environments, *Corrosion Science*, 39 (1998) 516-535.
- [17] B. Vuillemin, X. Philippe, R. Oltra, V. Vignal, L. Coudreuse, L.C. Dufour, E. Finot, SVET, AFM and AES study of pitting corrosion initiated on MnS inclusions by microinjection, *Corrosion Science*, 45 (2003) 1143-1159.
- [18] M. Khobaib, A. Rensi, T. Matakis, M.S. Donley, Real time mapping of corrosion activity under coatings, *Progress in Organic Coatings*, 41 (2001) 266-272.
- [19] D.J. Penney, J.H. Sullivan, D.A. Worsley, Investigation into the effects of metallic coating thickness on the corrosion properties of Zn-Al alloy galvanising coatings, *Corrosion Science*, 49 (2007) 1321-1339.
- [20] F. Thébault, B. Vuillemin, R. Oltra, K. Ogle, C. Allely, Investigation of self-healing mechanism on galvanized cut edges by coupling SVET and numerical modelling, *Electrochimica Acta*, 53 (2008) 5226-5234.
- [21] A. Bastos, M. Zheludkevich, M. Ferreira, Concerning the efficiency of corrosion inhibitors as given by SVET, *Portugaliae Electrochimica Acta*, 26 (2008) 47-54.

- [22] G. Williams, A.J. Coleman, H.N. McMurray, Inhibition of aluminium alloy AA2024-T3 pitting corrosion by copper complexing compounds, *Electrochimica Acta*, 55 (2010) 5947-5958.
- [23] J. Izquierdo, L. Nagy, J.J. Santana, G. Nagy, R.M. Souto, A novel microelectrochemical strategy for the study of corrosion inhibitors employing the scanning vibrating electrode technique and dual potentiometric/amperometric operation in scanning electrochemical microscopy: application to the study of the cathodic inhibition by benzotriazole of the galvanic corrosion of copper coupled to iron, *Electrochimica Acta*, 58 (2011) 707-716.
- [24] M. Mouanga, F. Andreatta, M.-E. Druart, E. Marin, L. Fedrizzi, M.-G. Olivier, A localized approach to study the effect of cerium salts as cathodic inhibitor on iron/aluminum galvanic coupling, *Corrosion Science*, 90 (2015) 491-502.
- [25] H. Shi, E-H. Han, F. Liu, T. Wei, Z. Zhu, D. Xu, Study of corrosion inhibition of coupled Al₂Cu–Al and Al₃Fe–Al by cerium cinnamate using scanning vibrating electrode technique and scanning ion-selective electrode technique, *Corrosion Science*, 98 (2015) 150-162.
- [26] T.H. Muster, A.E. Hughes, S.A. Furman, T. Harvey, N. Sherman, S. Hardin, P. Corrigan, D. Lau, F.H. Scholes, P.A. White, M. Glenn, J. Mardel, S.J. Garcia, J.M.C. Mol, A rapid screening multi-electrode method for the evaluation of corrosion inhibitors, *Electrochimica Acta*, 54 (2009) 3402-3411.
- [27] J. Zhang, G. Qiao, S. Hu, Y. Yan, Z. Ren, L. Yu, Theoretical evaluation of corrosion inhibition performance of imidazoline compounds with different hydrophilic groups, *Corrosion Science*, 53 (2011) 147-152.

- [28] G. Bereket, E. Hür, C. Öğretir, Quantum chemical studies on some imidazole derivatives as corrosion inhibitors for iron in acidic medium, *Journal of Molecular Structure: THEOCHEM*, 578 (2002) 79-88.
- [29] S. Sun, Y. Geng, L. Tian, S. Chen, Y. Yan, S. Hu, Density functional theory study of imidazole, benzimidazole and 2-mercaptobenzimidazole adsorption onto clean Cu (111) surface, *Corrosion Science*, 63 (2012) 140-147.
- [30] S.K. Saha, P. Banerjee, A theoretical approach to understand the inhibition mechanism of steel corrosion with two aminobenzonitrile inhibitors, *RSC Advances*, 5 (2015) 71120-71130.
- [31] S.K. Saha, A. Dutta, P. Ghosh, D. Sukul, P. Banerjee, Novel Schiff-base molecules as efficient corrosion inhibitors for mild steel surface in 1 M HCl medium: experimental and theoretical approach, *Physical Chemistry Chemical Physics*, 18 (2016) 17898-17911.
- [32] S. Kallip, A.C. Bastos, M.L. Zheludkevich, M.G.S. Ferreira, A multi-electrode cell for high-throughput SVET screening of corrosion inhibitors, *Corrosion Science*, 52 (2010) 3146-3149.
- [33] M. Talebian, K. Raeissi, M. Atapour, B.M. Fernández-Pérez, A. Betancor-Abreu, I. Llorente, S. Fajardo, Z. Salarvand, M. Amirnasr, R.M. Souto, Synthesis and evaluation of three new anionic Schiff bases as pitting corrosion inhibitor for stainless steel 304 in NaCl solution, *Electrochimica Acta*, submitted.
- [34] J. Izquierdo, B.M. Fernández-Pérez, L. Martín-Ruiz, V. Mena, R. Rodríguez-Raposo, J.J. Santana, R.M. Souto, Evaluation of the corrosion protection of steel by anodic processing

- in metasilicate solution using the scanning vibrating electrode technique, *Electrochimica Acta*, 178 (2015) 1-10.
- [35] M. Frisch, G. Trucks, H. Schlegel, G. Scuseria, M. Robb, J. Cheeseman, G. Scalmani, V. Barone, B. Mennucci, G. Petersson, Gaussian 09W, revision A. 02, Gaussian Inc, Wallingford, CT, 2009.
- [36] Y. Tang, X. Yang, W. Yang, R. Wan, Y. Chen, X. Yin, A preliminary investigation of corrosion inhibition of mild steel in 0.5 M H₂SO₄ by 2-amino-5-(n-pyridyl)-1,3,4-thiadiazole: polarization, EIS and molecular dynamics simulations, *Corrosion Science*, 52 (2010) 1801-1808.
- [37] I. Obot, N. Obi-Egbedi, E. Ebenso, A. Afolabi, E. Oguzie, Experimental, quantum chemical calculations, and molecular dynamic simulations insight into the corrosion inhibition properties of 2-(6-methylpyridin-2-yl)oxazolo[5,4-f][1,10]phenanthroline on mild steel, *Research on Chemical Intermediates*, 39 (2013) 1927-1948.
- [38] I. Obot, Z. Gasem, S. Umoren, Understanding the mechanism of 2-mercaptobenzimidazole adsorption on Fe (110), Cu (111) and Al (111) Surfaces: DFT and Molecular Dynamics simulations approaches, *International Journal of Electrochemical Science*, 9 (2014) 2367-2378.
- [39] S.K. Saha, A. Dutta, P. Ghosh, D. Sukul, P. Banerjee, Adsorption and corrosion inhibition effect of Schiff base molecules on the mild steel surface in 1 M HCl medium: a combined experimental and theoretical approach, *Physical Chemistry Chemical Physics*, 17 (2015) 5679-5690.

- [40] L. Li, X. Zhang, S. Gong, H. Zhao, Y. Bai, Q. Li, L. Ji, The discussion of descriptors for the QSAR model and molecular dynamics simulation of benzimidazole derivatives as corrosion inhibitors, *Corrosion Science*, 99 (2015) 76-88.
- [41] S. Kaya, B. Tüzün, C. Kaya, I.B. Obot, Determination of corrosion inhibition effects of amino acids: Quantum chemical and molecular dynamic simulation study, *Journal of the Taiwan Institute of Chemical Engineers*, 58 (2016) 528-535.
- [42] H. Sun, COMPASS: an ab initio force-field optimized for condensed-phase applications overview with details on alkane and benzene compounds, *The Journal of Physical Chemistry B*, 102 (1998) 7338-7364.
- [43] H. Sun, P. Ren, J.R. Fried, The COMPASS force field: parameterization and validation for phosphazenes, *Computational and Theoretical Polymer Science*, 8 (1998) 229-246.
- [44] E. McCafferty, Validation of corrosion rates measured by the Tafel extrapolation method, *Corrosion Science*, 47 (2005) 3202-3215.
- [45] M. Outirite, M. Lagrenée, M. Lebrini, M. Traisnel, C. Jama, H. Vezin, F. Bentiss, AC impedance, X-ray photoelectron spectroscopy and density functional theory studies of 3,5-bis(n-pyridyl)-1,2,4-oxadiazoles as efficient corrosion inhibitors for carbon steel surface in hydrochloric acid solution, *Electrochimica Acta*, 55 (2010) 1670-1681.
- [46] A.K. Singh, M. Quraishi, Investigation of the effect of disulfiram on corrosion of mild steel in hydrochloric acid solution, *Corrosion Science*, 53 (2011) 1288-1297.

- [47] J. Aljourani, M. Golozar, K. Raeissi, The inhibition of carbon steel corrosion in hydrochloric and sulfuric acid media using some benzimidazole derivatives, *Materials Chemistry and Physics*, 121 (2010) 320-325.
- [48] E. Oguzie, C. Enenebeaku, C. Akalezi, S. Okoro, A. Ayuk, E. Ejike, Adsorption and corrosion-inhibiting effect of *Dacryodis Edulis* extract on low-carbon-steel corrosion in acidic media, *Journal of Colloid and Interface Science*, 349 (2010) 283-292.
- [49] A.K. Singh, M. Quraishi, The effect of some bis-thiadiazole derivatives on the corrosion of mild steel in hydrochloric acid, *Corrosion Science*, 52 (2010) 1373-1385.
- [50] H. Amar, A. Tounsi, A. Makayssi, A. Derja, J. Benzakour, A. Outzourhit, Corrosion inhibition of Armco iron by 2-mercaptobenzimidazole in sodium chloride 3% media, *Corrosion Science*, 49 (2007) 2936-2945.
- [51] R. Solmaz, Investigation of adsorption and corrosion inhibition of mild steel in hydrochloric acid solution by 5-(4-dimethylaminobenzylidene)rhodanine, *Corrosion Science*, 79 (2014) 169-176.
- [52] J. Izquierdo, L. Martín-Ruíz, B.M. Fernández-Pérez, R. Rodríguez-Raposo, J.J. Santana, R.M. Souto, Scanning microelectrochemical characterization of the effect of polarization on the localized corrosion of 304 stainless steel in chloride solution, *Journal of Electroanalytical Chemistry*, 728 (2014) 148-157.
- [53] H. Amar, J. Benzakour, A. Derja, D. Villemin, B. Moreau, T. Braisaz, A. Tounsi, Synergistic corrosion inhibition study of Armco iron in sodium chloride by piperidin-1-yl-phosphonic acid–Zn²⁺ system, *Corrosion Science*, 50 (2008) 124-130.

- [54] H. Otmačić, E. Stupnišek-Lisac, Copper corrosion inhibitors in near neutral media, *Electrochimica Acta*, 48 (2003) 985-991.
- [55] H. Otmačić, J. Telegdi, K. Papp, E. Stupnišek-Lisac, Protective properties of an inhibitor layer formed on copper in neutral chloride solution, *Journal of Applied Electrochemistry*, 34 (2004) 545-550.
- [56] Y. Nakao, K.-I. Sakurai, A. Nakahara, Copper (II) chelates of Schiff bases derived from salicylaldehyde and various α -amino acids, *Bulletin of the Chemical Society of Japan*, 40 (1967) 1536-1538.
- [57] L.H. Abdel-Rahman, R.M. El-Khatib, L.A. Nassr, A.M. Abu-Dief, M. Ismael, A.A. Seleem, Metal based pharmacologically active agents: synthesis, structural characterization, molecular modeling, CT-DNA binding studies and in vitro antimicrobial screening of iron (II) bromosalicylidene amino acid chelates, *Spectrochimica Acta Part A: Molecular and Biomolecular Spectroscopy*, 117 (2014) 366-378.
- [58] B.-M. Kukovec, M. Kakša, Z. Popović, Synthesis and characterization of a copper (II) complex with 6-hydroxypicolinic acid and 3-picoline, *Croatica Chemica Acta*, 85 (2012) 479-483.
- [59] M. Costas, M.P. Mehn, M.P. Jensen, L. Que, Dioxygen activation at mononuclear nonheme iron active sites: enzymes, models, and intermediates, *Chemical Reviews*, 104 (2004) 939-986.

- [60] P.C. Bruijninx, G. van Koten, R.J.K. Gebbink, Mononuclear non-heme iron enzymes with the 2-His-1-carboxylate facial triad: recent developments in enzymology and modeling studies, *Chemical Society Reviews*, 37 (2008) 2716-2744.
- [61] J. Bolobajev, M. Trapido, A. Goi, Interaction of tannic acid with ferric iron to assist 2,4,6-trichlorophenol catalytic decomposition and reuse of ferric sludge as a source of iron catalyst in Fenton-based treatment, *Applied Catalysis B: Environmental*, 187 (2016) 75-82.
- [62] P.M. Boyer, C.P. Roy, J.M. Bielski, J.S. Merola, Pentamethylcyclopentadienylrhodium bis-carboxylates: monohapto carboxylate coordination, dihapto carboxylate coordination, and water coordination to Cp* Rh, *Inorganica Chimica Acta*, 245 (1996) 7-15.
- [63] J. Hu, D. Zeng, Z. Zhang, T. Shi, G.-L. Song, X. Guo, 2-Hydroxy-4-methoxyacetophenone as an environment-friendly corrosion inhibitor for AZ91D magnesium alloy, *Corrosion Science*, 74 (2013) 35-43.
- [64] V.S. Sastri, *Corrosion Inhibitors: Principles and Applications*, Wiley, New York, NY, 1998.
- [65] G. Gece, The use of quantum chemical methods in corrosion inhibitor studies, *Corrosion Science*, 50 (2008) 2981-2992.
- [66] R.G. Pearson, Absolute electronegativity and hardness: application to inorganic chemistry, *Inorganic Chemistry*, 27 (1988) 734-740.
- [67] R.M. Issa, M.K. Awad, F.M. Atlam, Quantum chemical studies on the inhibition of corrosion of copper surface by substituted uracils, *Applied Surface Science*, 255 (2008) 2433-2441.

- [68] K. Khaled, M.A. Amin, N. Al-Mobarak, On the corrosion inhibition and adsorption behaviour of some benzotriazole derivatives during copper corrosion in nitric acid solutions: a combined experimental and theoretical study, *Journal of Applied Electrochemistry*, 40 (2010) 601-613.
- [69] K. Khaled, Corrosion control of copper in nitric acid solutions using some amino acids—A combined experimental and theoretical study, *Corrosion Science*, 52 (2010) 3225-3234.
- [70] V. Sastri, J. Perumareddi, Molecular orbital theoretical studies of some organic corrosion inhibitors, *Corrosion*, 53 (1997) 617-622.
- [71] H.A. Rahman, A. Moustafa, M. Awad, Potentiodynamic and quantum studies of some amino acids as corrosion inhibitors for copper, *International Journal of Electrochemical Science*, 7 (2012) 1266-1287.
- [72] I. Lukovits, E. Kalman, F. Zucchi, Corrosion inhibitors—correlation between electronic structure and efficiency, *Corrosion*, 57 (2001) 3-8.
- [73] I. Ahamad, R. Prasad, M. Quraishi, Experimental and quantum chemical characterization of the adsorption of some Schiff base compounds of phthaloyl thiocarbohydrazide on the mild steel in acid solutions, *Materials Chemistry and Physics*, 124 (2010) 1155-1165.
- [74] D. Daoud, T. Douadi, H. Hamani, S. Chafaa, M. Al-Noaimi, Corrosion inhibition of mild steel by two new S-heterocyclic compounds in 1 M HCl: experimental and computational study, *Corrosion Science*, 94 (2015) 21-37.

- [75] I. Obot, D.D. Macdonald, Z. Gasem, Density functional theory (DFT) as a powerful tool for designing new organic corrosion inhibitors. Part 1: an overview, *Corrosion Science*, 99 (2015) 1-30.
- [76] A. Fouda, A. Ellithy, Inhibition effect of 4-phenylthiazole derivatives on corrosion of 304L stainless steel in HCl solution, *Corrosion Science*, 51 (2009) 868-875.
- [77] S.K. Saha, A. Hens, N.C. Murmu, P. Banerjee, A comparative density functional theory and molecular dynamics simulation studies of the corrosion inhibitory action of two novel N-heterocyclic organic compounds along with a few others over steel surface, *Journal of Molecular Liquids*, 215 (2016) 486-495.
- [78] H. Heydari, M. Talebian, Z. Salarvand, K. Raeissi, M. Bagheri, M.A. Golozar, Comparison of two Schiff bases containing O-methyl and nitro substitutes for corrosion inhibiting of mild steel in 1 M HCl solution, *Journal of Molecular Liquids*, Accepted manuscript (2018).

Figure captions**Figure 1**

Chemical structure of sodium (E)-4-(4-nitrobenzylideneamino)benzoate (SNBB).

Figure 2

E_{OCP} versus time curves for (a) F111 steel, (b) iron, and (c) copper immersed in 10 mM NaCl solution containing different concentrations of SNBB at 25 °C.

Figure 3

Potentiodynamic polarization curves recorded for (a) F111 steel, (b) iron, and (c) copper immersed in 10 mM NaCl solution containing different concentrations of SNBB at 25 °C; scan rate, 1 mV/s.

Figure 4

C_{inh}/θ versus C_{inh} plots obtained for (a) F111 steel, and (b) iron immersed in 10 mM NaCl solution containing various concentrations of SNBB at 25 °C.

Figure 5

SVET images and optical micrographs of grade F111 steel strips immersed in (a) 10 mM NaCl, and (b) 10 mM NaCl + 10 mM SNBB. The samples were left at their corresponding OCP values in the electrolyte for 60 min before starting to record the SVET images. Tip-substrate distance: 50 μm .

Figure 6

SVET images and optical micrographs of grade F111 steel strips immersed in (a) 10 mM NaCl, and (b) 10 mM NaCl + 10 mM SNBB. The steel samples were polarized at -0.10 V vs. Ag/AgCl/(3 M) KCl. Tip-substrate distance: 50 μm .

Figure 7

SVET images and optical micrographs of an iron–copper sample immersed in (a,c) 0.01 M NaCl, and (b,d) 0.01 M NaCl + 0.01 M SNBB. Electrical condition of the metal wires: (a,b) electrically insulated, i.e. each metal at its corresponding OCP value; (c,d) electrically connected to form a galvanic pair. The samples were left at their corresponding OCP values in the electrolyte for 60 min before starting to record the SVET images. Tip-substrate distance: 50 μm .

Figure 8

Sketches of the SNBB complexes formed on the (a) copper, and (b) the iron surfaces.

Figure 9

(a) Optimized structure, and electron density distributions of (b) HOMO and (c) LUMO levels in the SNBB inhibitor. They were obtained using the *B3LYP/6-311G*** methodology.

Figure 10

Top and side views of the equilibrium adsorption configurations of SNBB molecules on the (a,c) Fe (110), and (b,d) Cu (111) surfaces at 298 K obtained from MD simulations.

Table legends**Table 1**

Electrochemical parameters extracted from the potentiodynamic polarization curves recorded for Fe, F111 steel and Cu during immersed in 10 mM NaCl solution containing different concentrations of SNBB at 25 °C.

Table 2

Standard thermodynamic and equilibrium adsorption parameters for the adsorption of SNBB on the surface of pure iron and F111 steel immersed in 10 mM NaCl solution at 25 °C.

Table 3

Quantum chemical parameters for SNBB calculated using the *B3LYP/6-311G*** methodology.

Table 4

Comparison of the quantum parameters obtained for SNBB in this work with the values reported for other inhibitors in the literature.

Table 5

Interaction and binding energies obtained from MD simulations for the adsorption of SNBB on Fe (110) and Cu (111) surfaces at 298 K.

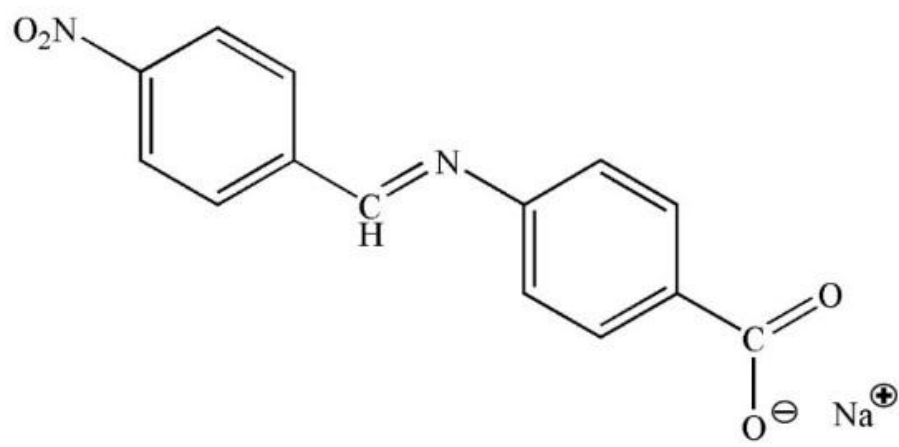


Figure 1

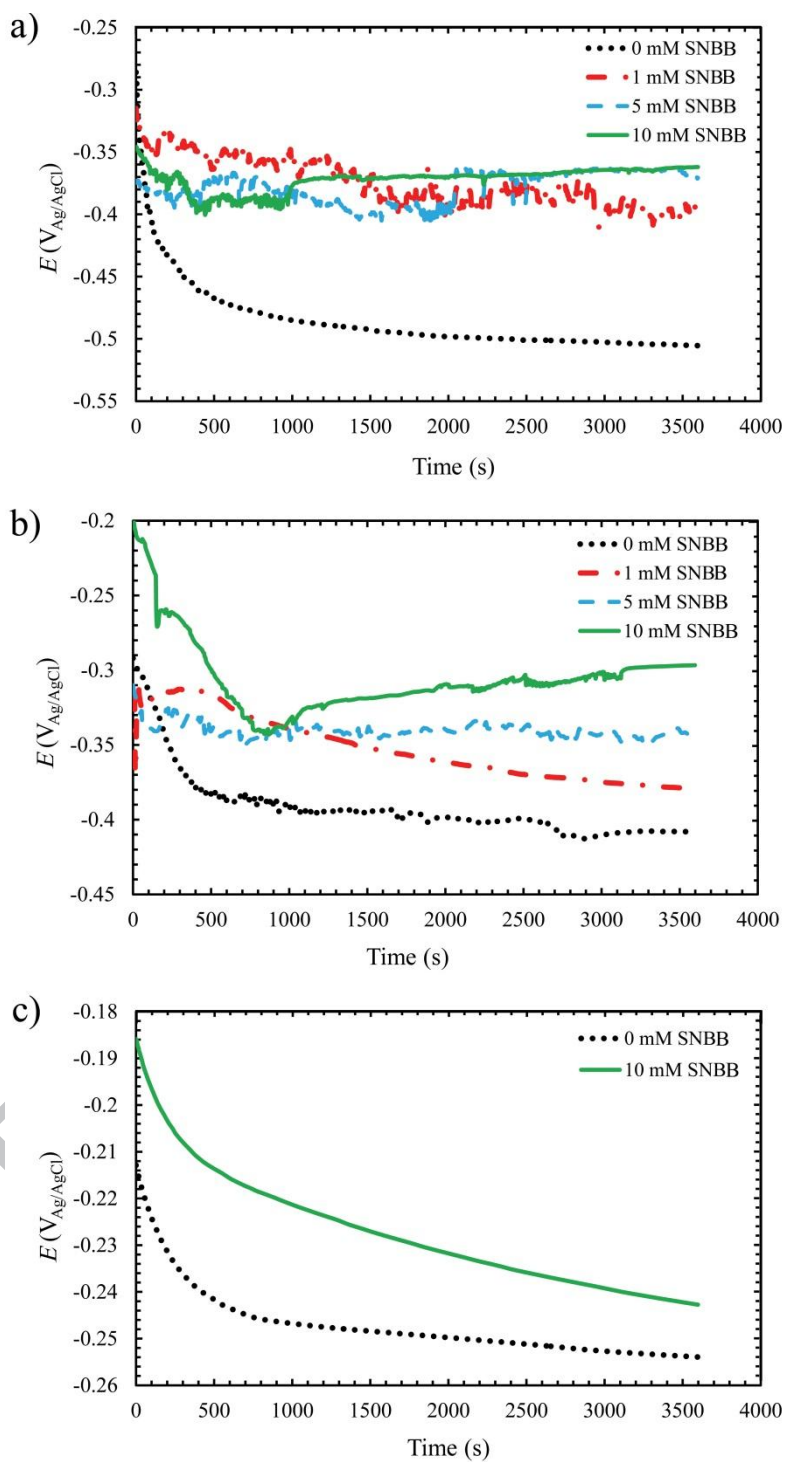


Figure 2

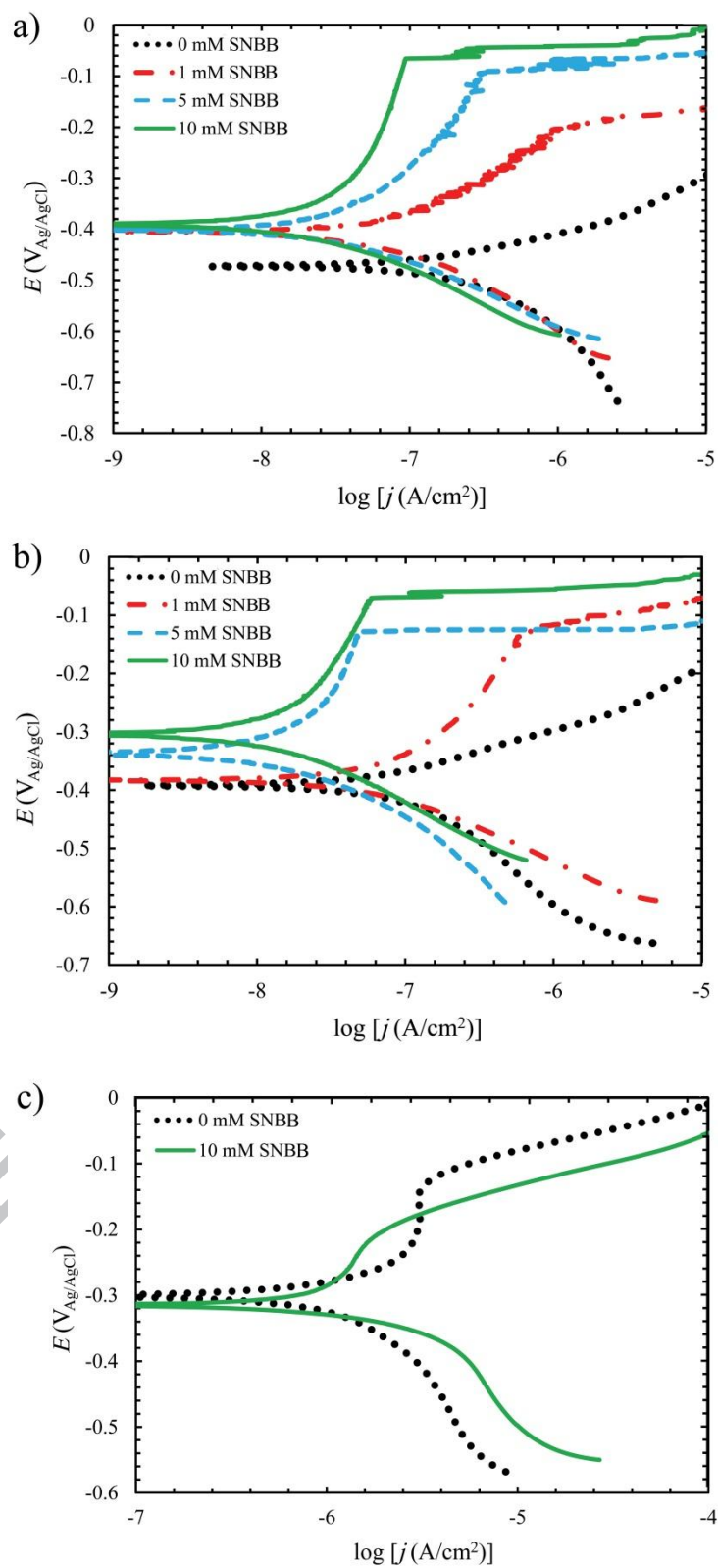


Figure 3

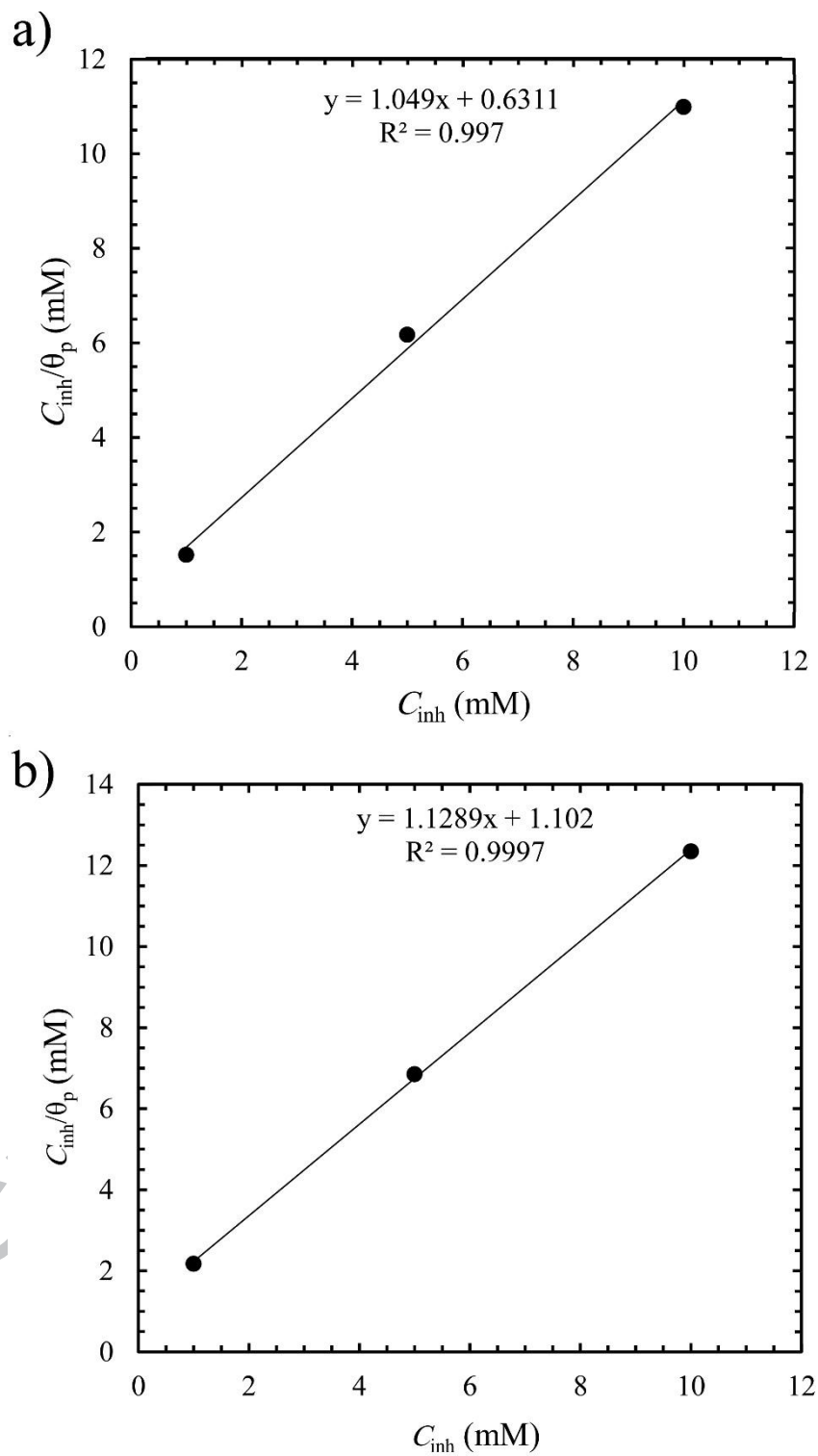


Figure 4

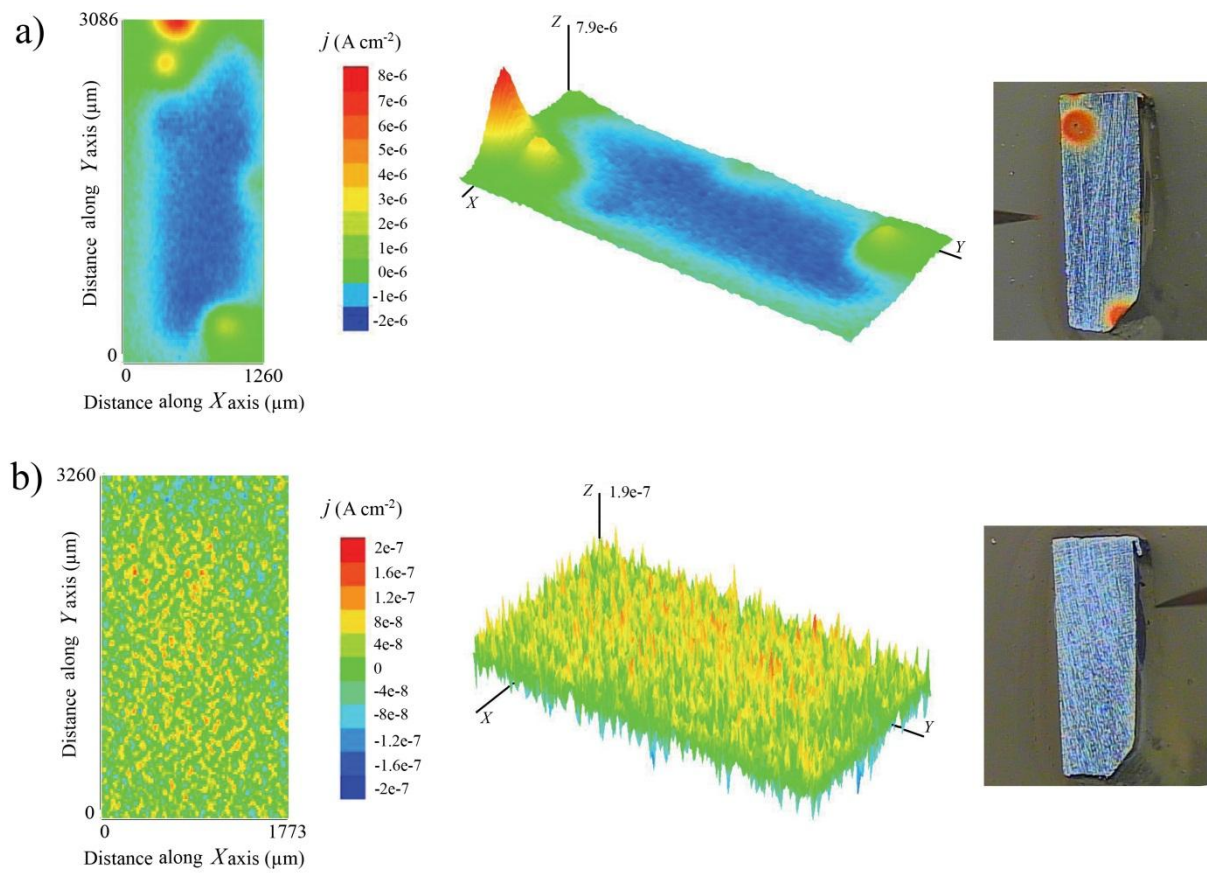


Figure 5

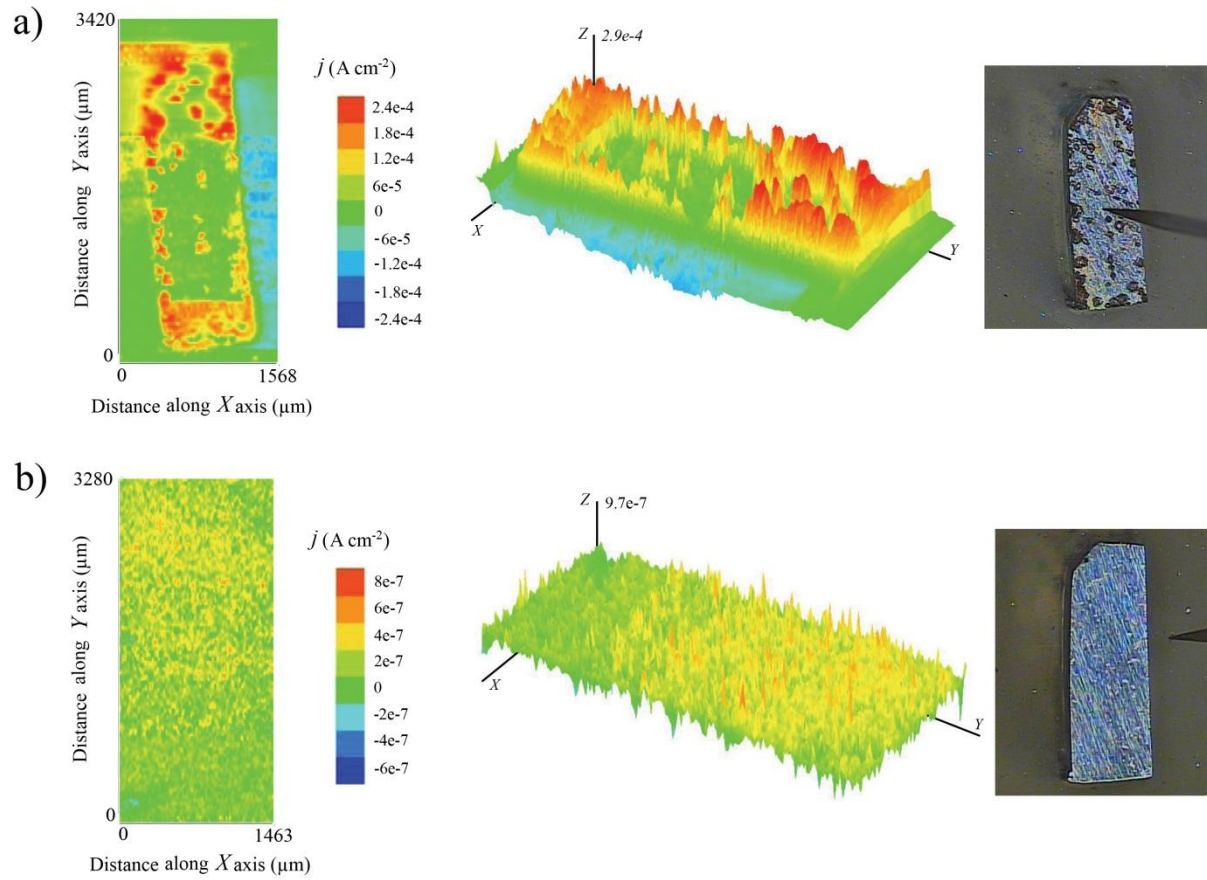


Figure 6

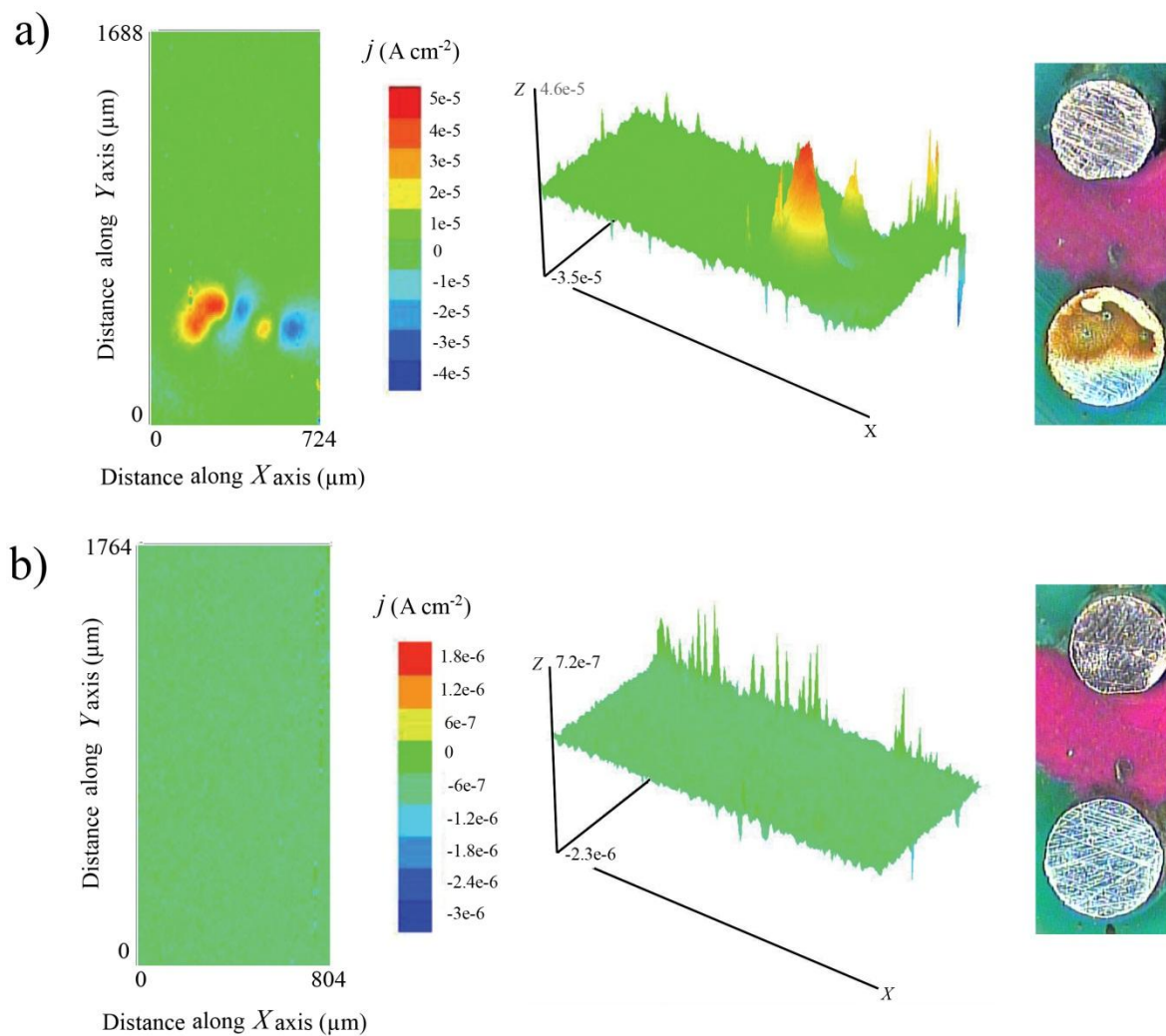


Figure 7

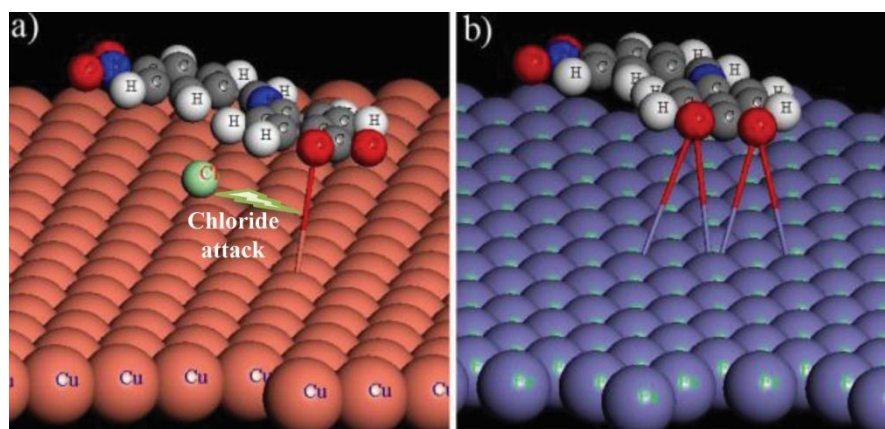


Figure 8

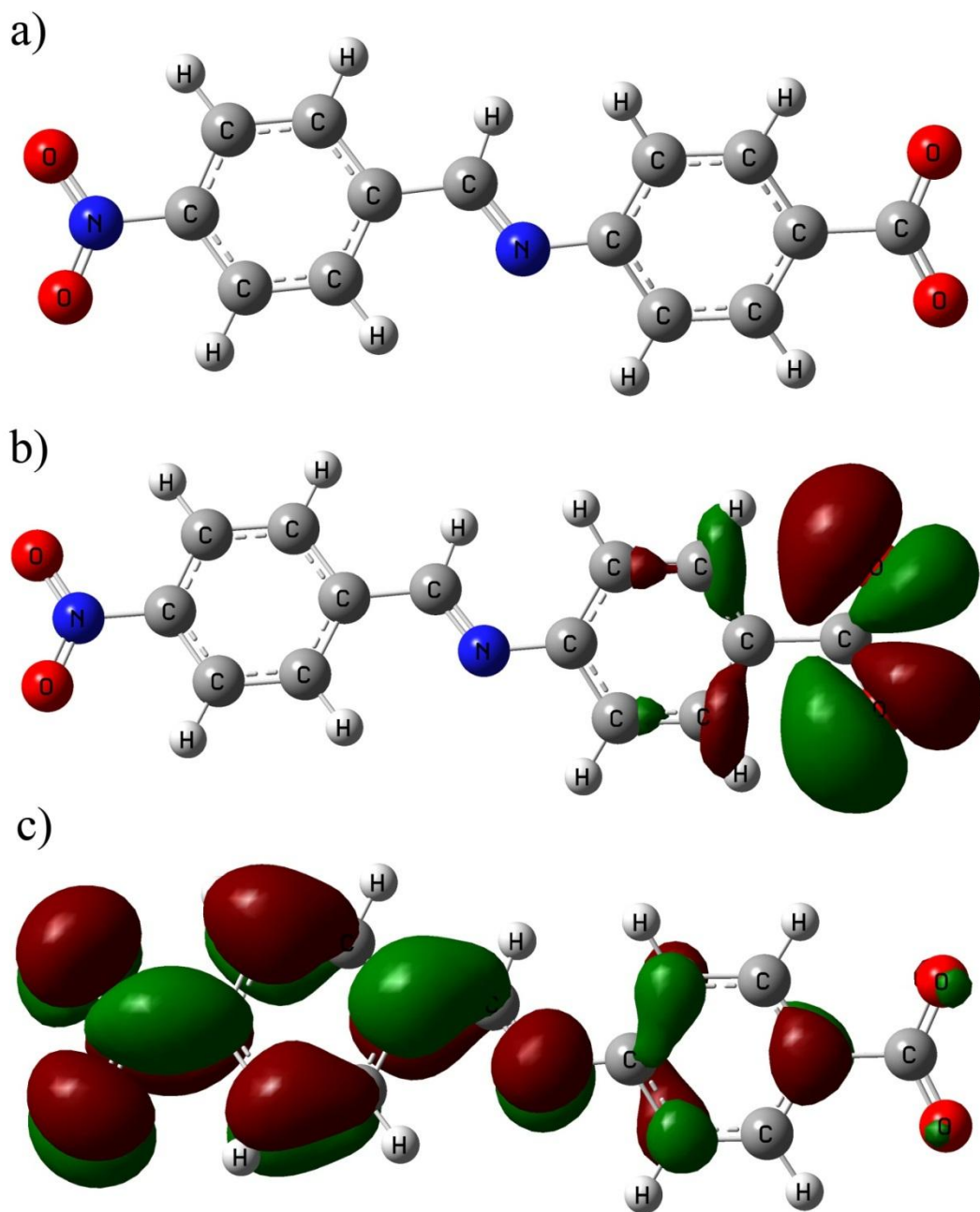


Figure 9

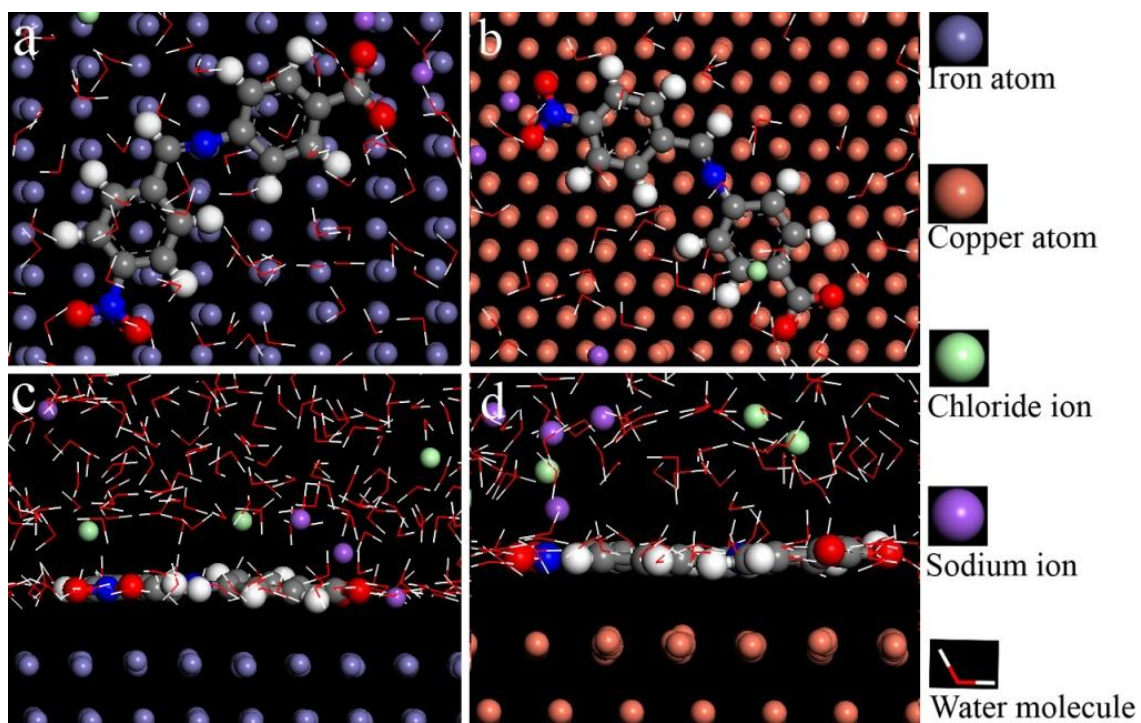


Figure 10

Table 1. Electrochemical parameters extracted from the potentiodynamic polarization curves recorded for Fe, F111 steel and Cu immersed in 10 mM NaCl solution containing different concentrations of SNBB at 25 °C.

Metal	C_{inh} (mM)	β_a (mV/dec)	β_c (mV/dec)	E_{corr} (mV vs. Ag/AgCl/(3 M) KCl)	j_{corr} (nA/cm ²)	$\eta_p\%$	θ_p
Fe	0	100	-141	-389	78	----	----
	1	144	-142	-379	42	46	0.46
	5	525	-148	-331	21	73	0.73
	10	435	-144	-305	15	81	0.81
F111	0	83	-145	-472	192	----	----
	1	169	-141	-410	65	66	0.66
	5	315	-135	-400	37	81	0.81
	10	701	-147	-385	17	91	0.91
Cu	0	301	-115	-252	1243	----	----
	10	344	-95	-245	1221	2	0.02

Table 2. Standard thermodynamic and equilibrium adsorption parameters for the adsorption of SNBB on the surface of pure iron and F111 steel immersed in 10 mM NaCl solution at 25 °C.

Metal	K_{ads} (L/mol)	$\Delta G^{\circ}_{\text{ads}}$ (kJ/mol)
Fe	2341	-26.37
F111	756	-29.17

ACCEPTED MANUSCRIPT

Table 3. Quantum chemical parameters for SNBB calculated using the *B3LYP/6-311G*** methodology.

$E_t(B3LYP)$	-25837.348 eV
E_{HOMO}	-2.25326 eV
E_{LUMO}	-1.3297 eV
ΔE	0.9235 eV
μ	19.2661 D
$\Delta N_{Fe^{2+}-inh}$	1.41
ΔN_{Cu^+-inh}	0.906

Table 4. Comparison of the quantum parameters obtained for SNBB in this work with the values reported for other inhibitors in the literature.

Inhibitor name	$E_{\text{HOMO}}(\text{eV})$	$\Delta E(\text{eV})$	Reference
Sodium (E)-4-(4-nitrobenzylideneamino)benzoate	-2.25	0.92	Current work
2-[2-(2-benzylidenehydrazine carbonothioyl)hydrazinecarbonyl]benzoic acid	-5.70	3.83	[73]
2-[2-{2-(2-hydroxybenzylidene)hydrazinecarbonothioyl}hydrazinecarbonyl]benzoic acid	-5.70	3.83	[73]
2-[2-{2-(2-hydroxy-4-methoxybenzylidene)hydrazinecarbonothioyl}hydrazinecarbonyl]benzoic acid	-5.70	3.83	[73]
Indole	-8.35	8.53	[76]
benzotriazole	-8.89	8.32	[76]
benzothiazole	-9.24	8.50	[76]
benzoimidazole	-9.31	9.24	[76]
2-aminobenzonitrile	-5.90	4.59	[30]
3-aminobenzonitrile	-5.79	4.39	[30]
Neutral Red	-5.86	2.73	[77]
Azure A Eosinate	-6.10	2.49	[77]
Toluidine Blue	-6.05	2.47	[77]
Phenosafranin	-6.13	2.88	[77]
N-(4-methoxybenzylidene)-2-[2-((E)-2-(4-methoxybenzylideneamino)phenyl)disulfanyl]benzenamine	-5.72	3.75	[78]
N-(4nitrobenzylidene)-2-[2-((E)-2-(4-nitrobenzylideneamino)phenyl)disulfanyl]benzenamine	-6.44	4.10	[78]
1H-benzoimidazole	-7.56	5.52	[40]
2-(chloromethyl)-1H-benzoimidazole	-8.99	6.43	[40]
2-(pyridin-2-yl)-1H-benzoimidazole	-7.27	4.39	[40]
2-amino-N,N-dihydroxy-3H-benzoimidazol-4-amine	-7.33	3.87	[40]
N,N-dimethyl-3H-benzoimidazole-2,4-diamine	-6.86	5.77	[40]
N,N-dimethyl-3H-benzoimidazole-2,5-diamine	-7.04	5.99	[40]
N,N-dihydroxy-3H-benzoimidazol-4-amine	-8.28	6.41	[40]
(1H-benzo[d]imidazol-2-yl)methanethiol	-7.64	5.67	[40]
N,N-dihydroxy-3H-benzoimidazol-5-amine	-8.29	4.89	[40]
2-amino-N,N-dihydroxy-3H-benzoimidazol-5-amine	-7.40	4.17	[40]
1-(1H-benzo[d]imidazol-2-yl)hydrazine	-9.07	7.86	[40]
2-chloro-1H-benzoimidazole	-10.39	8.21	[40]
1H-benzoimidazol-2-ol	-10.52	8.99	[40]
1H-benzoimidazole-2-carbonitrile	-10.23	8.44	[40]
1-methyl-1H-benzoimidazol-2-amine	-9.66	8.41	[40]
1-methyl-2-(methylthio)-1H-benzoimidazole	-7.42	5.60	[40]
1H-benzoimidazol-2-amine	-10.38	9.12	[40]
1H-benzoimidazole-2-thiol	-10.40	8.47	[40]
(1H-benzo[d]imidazol-2-yl)methanol	-10.34	8.44	[40]

N,N-dimethyl-1H-benzoimidazol-4-amine

-8.09

6.18

[40]

ACCEPTED MANUSCRIPT

Table 5. Interaction and binding energies obtained from MD simulations for the adsorption of SNBB on Fe (110) and Cu (111) surfaces at 298 K.

Systems	$E_{\text{adsorption}}$ (kJ/mol)	E_{binding} (kJ/mol)
Fe (110) + SNB	-564.05	564.05
Cu (111) + SNB	-288.90	288.90

ACCEPTED MANUSCRIPT